UC Davis

UC Davis Previously Published Works

Title

Antiferromagnet thickness dependence and rotatable spins in exchange biased CoO/Fe films

Permalink

https://escholarship.org/uc/item/6x36m27r

Authors

Greene, Peter K
Hu, Yong
Qiu, Ziqiang
et al.

Publication Date

2022-12-01

DOI

10.1016/j.jmmm.2022.169898

Peer reviewed

eScholarship.org Powered by the California Digital Library
University of California

Antiferromagnet Thickness Dependence and Rotatable Spins in Exchange Biased CoO/Fe Films

Peter K. Greene,[1] Yong Hu,[1,2] Ziqiang Qiu,[3] and Kai Liu[1,4*]

[1]*Physics Department, University of California, Davis, CA 95616, USA*

[2]*College of Sciences, Northeastern University, Shenyang 110819, China*

[3]*Physics Department, University of California, Berkeley, CA 94720, USA*

[4]*Physics Department, Georgetown University, Washington, DC 20057, USA*

Abstract

The emergence of exchange bias and coercivity enhancement has been investigated in epitaxial CoO/Fe films with varied antiferromagnet (AF) thicknesses, even smaller than the critical value where the frozen CoO spins are detectable. Vector magnetometry and first-order reversal curve (FORC) measurements reveal different CoO thickness dependence of the exchange bias and coercivity enhancement, including the evolution of magnetization reversal from a high coercivity, low bias phase due to rotatable CoO moments to a high bias, low coercivity phase due to frozen CoO moments. The AF domain state is found to be metastable, which can be reoriented by external and exchange fields prior to the appearance of frozen spins. Monte Carlo simulations show that the AF anisotropy energy barrier and the rotatable spins induced by magnetic field and exchange interaction at the interface are responsible for the observed effects.

Introduction

The proximity effect between an antiferromagnet (AF) and a ferromagnet (FM) known as exchange bias has been an intriguing topic of research since its discovery in 1956 by Meiklejohn and Bean.[1] This effect is based on the unidirectional character of the exchange interaction at the FM/AF interface, breaking the time-reversal symmetry of the interaction between the external field and the magnetic moment.[2-5] It has important applications in spin-valve type of devices which are central to numerous spintronic applications.[6-10] Indeed, there has been a surge of interests recently on electric field control of exchange bias with potentials to lower the energy consumption in spintronic devices.[11-18]

Although it is well acknowledged that the existence of the AF layer induces the exchange bias and coercivity enhancement in the FM layer, the microscopic correlation between the exchange bias and the AF order is often masked by the complex magnetic frustration at the FM/AF interface and the difficulty in experimental detection of the net zero magnetization in the AF layer.[2-5, 19-21] On the other hand, the Meiklejohn and Bean theory has been extended to describe the critical AF thickness behavior, but with limitations on quantitatively predicting the exchange field value.[22] An alternate theory was proposed by Mauri *et al.*[23] showing that a rotation of the magnetization accompanied by partial wall formation in the AF layer can substantially reduce the exchange and that the peak in the bias dependence on AF thickness could be explained by introducing a vertical domain wall in the AF layer. By strongly coupling the FM layer to the AF layer, the FM magnetization reversal winds up a region of the AF layer into a partial domain wall, which has been probed in a number of experiments.[24-26] Stiles and McMichael[27] have extended the modeling of AF domain wall formation in polycrystalline systems by

taking into account various sample scenarios. Most studies imply or explicitly state that any irreversible switching within the AF layer is confined very close to the interface. Experimental and theoretical results in the FM/diluted AF bilayers and the FM/AF/FM trilayers have shown that the strength of the bias and the coercivity enhancement are also determined by spins deep inside the AF layer.[21, 28-32]

Recently, a series of experimental investigations on the CoO/Fe interface have been reported related to the CoO thickness dependence, ranging from the exchange bias mechanism,[33, 34] to the AF anisotropy[35, 36] and domain,[37, 38] and to the influence of interface chemical interactions on magnetic and structural properties.[39] The behavior of the CoO AF spins as a function of thickness has been directly investigated using element-specified x-ray magnetic linear dichroism (XMLD) and x-ray magnetic circular dichroism (XMCD).[33-35, 37] It has been shown that rotatable and frozen CoO AF spins are uniformly distributed in the AF layer and interestingly, the appearance of exchange bias occurs *prior* to the detection of the frozen AF spins.[33] Furthermore, the uniaxial anisotropy and the CoO frozen spins are found to exhibit the same CoO thickness dependence, and the relation between the CoO activation energy and thickness is linear when the CoO thickness is larger than 2.2 nm.[35] It has also been reported that a CoO domain switching occurs with the increase of the CoO thickness.[37] Note that the CoO with this transitional thickness has a reduced effective Néel temperature due to the finite-size effect.[19]

Remarkably, for the thin CoO layer (< 3.0 nm approximately), the exchange bias, coercivity enhancement, CoO anisotropy and frozen spins depend differently on the CoO layer thickness. The phenomenological interpretations based on the theories of the AF uncompensated and frozen spins at the FM/AF interface are no longer suitable in these studies. In this work, we have investigated the emergence

of exchange bias and coercivity enhancement in epitaxial CoO/Fe with increasing CoO thickness, as the interfacial AF spins transition from being rotatable to completely frozen. Vector magnetometry and the first-order reversal curve (FORC) technique have been used to measure the magnetization reversal details and separate the reversible and irreversible magnetic switching events. An atomic Monte Carlo technique has been used to simulate hysteresis loops and magnetic energies as a function of the AF layer thickness. The AF anisotropy energy barrier and the rotatable spins induced by magnetic field and exchange interaction at the FM/AF interface, as a function of the AF layer thickness, both influence exchange bias and coercivity through direct interface coupling and indirect Néel-Arrhenius relaxation in the AF layer.

Experimental

Samples were fabricated by molecular beam epitaxy (MBE) in an ultrahigh vacuum system. Sample structures consist of MgO(001) substrate/Fe(10nm)/CoO(d_{CoO})/Ag(10nm), where the CoO is an epitaxial wedge from 0 to 4 nm over a sample width of 6 mm, followed by a 6 nm CoO plateau over a width of 4 mm.[33, 35] The Fe grows epitaxially onto MgO(001) with the Fe [110] parallel to the MgO [100],[33, 35] and exhibits a cubic magnetic anisotropy with the <100> axes as the magnetic easy axes. The samples were then cleaved into 0.9 mm strips, resulting in a CoO thickness variation of 0.6 nm across each cut wedge piece. CoO has a NaCl type face-centered cubic lattice, with a lattice constant of a_0=0.426 nm;[19] thus there is approximately a three-monolayer variation of CoO across each cut sample piece (each monolayer ~ 0.2nm).

Samples were field cooled from room temperature, above the CoO Néel temperature of 290 K, to 80 K in a 2 kOe external field along the Fe [100] direction for all measurements. VSM measurements were performed with vector coils in the plane of the film along the Fe [100] and Fe [010] directions at 80 K. The FORC technique[40-44] was utilized to further investigate the magnetization reversal along the Fe [100] and Fe [010] directions, particularly to probe irreversible switching events. During the measurement, the sample was first brought from positive saturation to a reversal field H_R, then the magnetization was measured as a function of increasing applied field H, back to saturation. This process was repeated for a family of H_R values yielding the magnetization as a function of both the reversal field H_R and the applied field H. The FORC distribution is calculated by taking the mixed second order derivative of the magnetization,[40]

$$\rho(H, H_R) = -\frac{1}{2}\frac{\partial^2 M(H,H_R)}{\partial H \partial H_R}. \quad (1)$$

By identifying reversal field H_R and applied field H as the switch-down and switch-up field, respectively, a coordinate transformation is performed to arrive at a FORC distribution in new coordinates of bias field H_B=(H+H_R)/2 and local coercivity H_C=(H-H_R)/2. These coordinates correspond to the offset of the loop from center (H_B) and the half width of the loop (H_C), respectively. Features in the FORC distribution correspond to irreversible switching events, consequently revealing details about the magnetization reversal and local interactions within each sample.[41, 43, 45] For example, if the entire sample switched exactly at a particular reversal field, the FORC distribution would be a delta function. However, if different regions of the sample experience different local environments, the distribution will spread out.[46] In this way the extent of the FORC distribution can be used to evaluate the rotatable and pinned CoO spins as a function of the CoO layer thickness.

Theoretical Model

To further understand the dependence of exchange bias and coercivity on the AF thickness d_{CoO}, simulations using an atomic Monte Carlo method have been carried out. The simulation procedure mimics the experiments. Different from many previous theoretical studies on the AF thickness dependence which commonly linked the exchange bias with the AF domain,[32, 47-50] the AF anisotropy energy barrier induced at the FM/AF interface is considered to be crucial and calculated to interpret the results in the present study where the AF layer may be too thin to form a complete AF domain. In the presence of an external magnetic field, the energy of the system with interacting spins can be given as follows,

$$E = E_{\mathrm{FM}} + E_{\mathrm{IF}} + E_{\mathrm{AF}}, \tag{2}$$

where

$$E_{\mathrm{FM}} = -J_{\mathrm{FM}} \sum_{<ij\in \mathrm{FM}>} \mathbf{S}_i \cdot \mathbf{S}_j - \sum_{i\in \mathrm{FM}} [K_i^x (S_i^x)^4 + K_i^y (S_i^y)^4] - \sum_{i\in \mathrm{FM}} K_i^z (S_i^z)^2 - g\mu_{\mathrm{B}} \mathbf{H} \cdot \sum_{i\in \mathrm{FM}} \mathbf{S}_i , \tag{3}$$

$$E_{\mathrm{IF}} = -J_{\mathrm{IF}} \sum_{<i\in \mathrm{FM},\, j\in \mathrm{AF}>} \mathbf{S}_i \cdot \mathbf{S}_j , \tag{4}$$

$$E_{\mathrm{AF}} = -\delta J_{\mathrm{AF}} \sum_{<ij\in \mathrm{AF}>} \mathbf{S}_i \cdot \mathbf{S}_j - \sum_{i\in \mathrm{AF}} K_i^x (S_i^x)^2 - g\mu_{\mathrm{B}} \mathbf{H} \cdot \sum_{i\in \mathrm{AF}} \mathbf{S}_i . \tag{5}$$

Here **S** is the unit vector of classical Heisenberg spin. We consider the exchange and Zeeman energies, as well as cubic and shape anisotropies in the FM layer (E_{FM}), along with exchange, Zeeman and uniaxial anisotropy energies in the AF layer (E_{AF}). If the spins in the FM (AF) layer are exchange coupled to the spins in the AF (FM) layer, these spins belong to the FM/AF interface (E_{IF}). Different parameters are used to distinguish the FM and AF layers, as listed in Table 1. Note that p is a probability of obtaining δ=1. If p=0, the nearest-neighbor spins in the AF layer are decoupled to each other; on the contrary, if p=1, all the spins in the AF layer are coupled to their nearest neighbors antiferromagnetically. As

concomitant effects with the increase of d_{CoO}, the AF anisotropy increases and the AF order is enhanced (i.e. *p* increases).[51, 52] The relationship between *p* and d_{CoO} is unknown, and thus for simplicity, *p* and AF anisotropy both linearly increase with d_{CoO} and the parameter values are determined by magnetometry measurements. In the model, the spins are placed on the node of a simple cubic lattice, and the 100×100 spins with periodic boundary conditions are considered in a monolayer of the film plane. Open boundary conditions are used perpendicular to the film plane. The FM layer is one-monolayer, while various AF layer thicknesses are considered, including 0- (the FM single layer), 1- (thin AF) and 7-monolayer (thick AF).

In the experiment, the initial temperature is room temperature, well below the Fe Curie temperature. For the CoO/Fe bilayers with a small d_{CoO}, the cooling field of 2 kOe is strong enough to saturate the system at 80 K. Therefore, no additional cooling process is considered in the simulations. The measuring field is applied on the system with an initial state where the spins are all pointing to the positive *x* axis. The hysteresis loops are recorded between 2.0 $J_{FM}/g\mu_B$ and -2.0 $J_{FM}/g\mu_B$ in a step of 0.04 $J_{FM}/g\mu_B$. Under a magnetic field, the simulation time is represented by Monte Carlo steps. A total of 10^5 Monte Carlo steps are used to equilibrate the system, succeeded by another 10^5 Monte Carlo steps for averaging magnetization and energy quantities. Furthermore, the results are averaged over 200 independent realizations of randomly generated trial spin configurations to minimize statistical errors.

Results and Discussion

Magnetometry

Magnetic hysteresis loop measured along the Fe [100] direction (Fig. 1) shows that the exchange bias first emerges in a sample with a CoO thickness of d_{CoO}=1.5±0.3 nm, and further increases in magnitude to -175 Oe at d_{CoO} =3.3 nm, before gradually decreasing with further increase of d_{CoO}, consistent with prior studies on this system.[33] The coercivity increases to a maximum at d_{CoO}~1.5±0.3 nm and then decreases. Note that the hysteresis loops for d_{CoO}<3.0 nm (Figs. 1a-c) have asymmetric descending and ascending field branches. The descending branch exhibits a sharp reversal for all but the thinnest CoO while the ascending branch has a rounded up-turn and a more gradual approach toward saturation. This effect is most notable for d_{CoO}=1.8-2.4 nm (Fig. 1b), similar to what was predicted by Mauri *et al*.[23] for a domain wall introduced into the AF layer and indicative of irreversible events within the CoO.

Subsequently the sample was rotated by 90° so the applied field was along the Fe [010] direction. Vector coil loops were measured along the Fe [010] and [100] directions (Fig. 2 schematic). The Fe [010] direction (Fig. 2, solid circles) shows a gradual evolution into a hard axis type loop at a CoO thickness of 2.7±0.3 nm. For the thinnest CoO samples (Figs. 2a-b) the loops exhibit a single step reversal. However, for larger CoO thicknesses the hysteresis loop evolves into two sub-loops (Figs. 2c-d); above d_{CoO}=2.4 nm (Fig. 2e) the hysteresis is largely suppressed, indicating mostly reversible magnetization switching.

The Fe transverse magnetization along the [100] direction (Fig. 2, open circles) initially follows a multiple domain reversal mode at d_{CoO}=0-0.6 nm (panel a), with opposite peaks along descending and ascending field branches whose magnitudes are well below the saturation magnetization. At d_{CoO}=0.6-1.2 nm (Fig. 2b), the transverse peaks shift to the same side, due to the exchange bias breaking the

rotational symmetry of the sample and the moments preferentially rotate in the exchange bias direction. However, the rotation is not fully coherent as evidenced by the lack of saturation along Fe [100]. Interestingly, this effect emerges just as the exchange bias is being established. For d_{CoO}=1.2-2.4 nm (Figs. 2c-d) the transverse magnetization is saturated in the Fe [100] direction, indicating a coherent rotation of the Fe into the field cooling direction, yet hysteresis remains. This suggests that the magnetocrystalline cubic Fe [110] energy barrier makes the Fe [010] and Fe [$0\bar{1}0$] directions metastable states. At d_{CoO}>2.4 nm the hysteresis in the Fe transverse magnetization largely vanishes (Fig. 2e, open circles), corresponding to the exchange field overcoming the magnetocrystalline Fe [110] energy barrier, leaving only the Fe [100] as a stable energy minima.

FORC analysis

To better understand details of the magnetization reversal, FORC measurements were performed with the applied field along the Fe [100] and [010] directions, while field cooling was always performed along the Fe [100] direction, as shown in Fig. 3. Magnetization in the FORCs was always measured parallel to the applied field. The FORC distributions map out irreversible switching events within the sample with the peak of the feature at the dominant loop characteristic.[41, 53] Note that the center of the FORC features corresponds to most prominent distributions of the microscopic bias field and local coercivity, which are often correlated with, but not necessarily the same as those from the major hysteresis loop. The FORC distributions clearly show the previously seen trends in both bias and coercivity. Furthermore, the extents of the distributions reveal more detail about the behavior of the samples.

As expected, the sample with no CoO (i.e., just the Fe film) exhibits very sharp FORC distributions with low coercivity and zero bias, and no difference between measurement directions (Figs. 3a-b). For the smallest amount of CoO deposited (0-0.6 nm) (Figs. 3c-d) the FORC distribution is centered on (H_C=60 Oe, H_B=0 Oe), with the feature spread out along the coercivity axis. This shows that ~1.5 monolayer of CoO is enough to hinder the reversal of the Fe film, yet not enough to establish bias or to break the four-fold symmetry of the Fe film.

At a thickness of d_{CoO}=0.6-1.2 nm, the FORC distribution measured along the Fe [100] direction (Fig. 3e) shifts to a yet higher coercivity and finite bias, centered at (H_C=130 Oe, H_B= -10 Oe). The distribution measured along the Fe [010] direction (Fig. 3f, arrow) shows the development of "tails" off the main feature extending in the bias direction. This occurs as the vector coil loops show the four-fold symmetry of the Fe being broken by the exchange field induced by the CoO along the field cooling direction (Fig. 2b), causing the Fe to preferentially reverse through the Fe [100] direction.

For d_{CoO}=1.2-1.8 nm a drastic change in the reversal behavior is observed as two separate FORC features are observed. The Fe [100] FORC distribution exhibits a larger spread in coercivity of the main feature (H_C=150 Oe, H_B= -100 Oe), than any other samples (Fig. 3g). The spread of the main feature along the bias direction also increases significantly. There is a second, lower intensity peak at smaller bias and larger coercivity (H_C=225 Oe, H_B= -35 Oe) (Fig. 3g, dashed circle), showing two distinct phases coexist within the sample at this thickness range. The placement and spread of these features provide interesting insight into the transition from rotatable to pinned CoO moments. *The coexistence of a high bias, low coercivity phase alongside a high coercivity, low bias phase strongly suggests the transition from mostly rotatable CoO moments that lead to the high coercivity phase to frozen CoO moments*

pinning a large bias, lower coercivity phase. At this thickness the vector coil loops show the Fe film coherently rotating into the Fe [100] direction during reversal (Fig. 2c), confirming the existence of pinned CoO moments. The FORC distribution along the Fe [010] direction (Fig. 3h) shows the feature split into three distinct peaks, a pair at H_C=150 Oe, roughly symmetric about the H_C axis, and a third peak at (H_C=280 Oe, H_B~0 Oe). The observations of these peaks are due to the existence of three local energy minima of the magnetization, corresponding to the crystalline states of Fe [010], Fe [100], and Fe [$0\bar{1}0$]. They arise because the CoO exchange energy is not strong enough to overcome the in-plane crystalline energy barriers as corroborated by the aforementioned vector coil measurements.

When the CoO thickness reaches 1.8-2.4 nm the Fe [100] FORC distribution is centered at (H_C=135 Oe, H_B= - 145 Oe) (Fig. 3i), showing an even higher bias value. The FORC feature has smaller spread than the 1.2-1.8 nm CoO sample, indicating tighter variations of exchange energy across the width of the sample as well as the feature coalescing into the single high bias phase. The vector coils and the Fe [010] FORC (Fig. 3j) show qualitatively similar features to the previous sample with the same physical interpretations. The separation between the peaks in the vector coil Fe [010] peaks is smaller than previous measurements on thinner CoO samples and the peak separation of the low coercivity features in the Fe [010] FORC distribution are larger (Fig. 3j, dashed circle). The low coercivity peaks in the Fe [010] FORC arise as a consequence of the applied field required to overcome the crystalline and exchange induced energy barrier. Consequently, the larger the spread between the low coercivity peaks, the larger the exchange field, as the crystalline energy barrier can be considered constant. The high coercivity peak (Fig. 3j, arrow) in the Fe [010] distribution arises from the existence of multiple stable magnetization states at H=0.

For d_{CoO}=2.4-3.0 nm the Fe [100] FORC distribution is shifted to (H_C=110 Oe, H_B= -170 Oe) (Fig. 3k) and its spread shrinks, indicating only slight variation in exchange bias across the sample and revealing a weak thickness dependence. In the corresponding Fe [010] FORC diagram (Fig. 3l) the high coercivity feature disappears due to the fact that there is only one zero applied field stable magnetization state. In other words, the exchange field can now overcome the crystalline energy barriers and there is no longer hysteresis at zero applied field. Likewise, there is no longer significant hysteresis in the vector coil loops with field along the Fe [010] direction (Fig. 2e).

At a CoO thickness of greater than 3.0 nm the FORC distributions are very similar. The Fe [100] FORC distribution (Fig. 3m) shows a very narrow feature centered at (H_C=100 Oe, H_B= -160 Oe) for d_{CoO} = 3.0 - 3.6 nm. Likewise, only two low coercivity features are observed in the corresponding Fe [010] FORC distribution (Fig. 3n). These features are consistent for all CoO thickness larger than 3.0 nm, the only difference being the evolution of the FORC features towards smaller absolute values of both the coercivity and bias.

When considering the meaning of FORC distributions one must take into account both the peak position and the spread of the features to obtain a full picture of the reversal. The spread in the FORC features arises from a convolution of independent regions exhibiting different local coercivities, interactions within the CoO/Fe film, and irreversible changes within the CoO. Figure 4 shows the evolution of the Fe [100] FORC distributions, integrated along the bias (solid circles) and coercivity (solid squares) axes and the peak positions in H_C and H_B are plotted along with the half-width-at-half-maximum (HWHM) (Fig. 4, open symbols) of the integrated feature.

Starting from the left of Fig. 4 at d_{CoO}=0 the feature exhibits very low coercivity and a very small HWHM in both the H_B and H_C directions. This provides a reference for a stand-alone Fe layer that switches rather uniformly and abruptly. When a 0-0.6 nm layer of CoO is added to the sample, the coercivity and spread in both H_B and H_C increase. This indicates that the CoO interfacial moments are impeding the domain wall motion, likely by causing local pinning fields. Yet, the CoO moments are still fully rotatable even with more than a full monolayer of CoO. As the CoO thickness increases to d_{CoO}=0.6-1.2 nm, the first measurable bias is observed, the coercivity increases substantially, and the spread of the FORC feature along the coercivity axis is maximal. The small bias and relatively small spread of the FORC feature in the bias direction indicate that most of the sample has no pinned CoO moments, or the anisotropy in CoO is too weak to provide sufficient pinning.[54] The bias is most likely due to the thickest edge of the sample at d_{CoO}=1.2 nm, supported by the facts that the sample is only partially reversing via the field cooling direction as an intermediate state (Fig. 2b, open circles) and the similarities between the FORCs performed along the Fe [100] and Fe [010] directions (Figs. 3e-f). However, the very large coercivity and large spread in the coercivity indicates a rapid change in the interaction strengths within this thickness range. While the CoO moments are nearly completely free to rotate, there is a rapid increase in the CoO anisotropy with thickness, thereby stabilizing the underlying Fe film against the external field.[52]

For d_{CoO}>1.2 nm the samples start to exhibit a new reversal pattern. The rapid onset of bias is observed along with a maximum spread in the bias projection of the FORC feature. For the first time in this series, no part of the FORC feature extends over the coercivity axis (along H_B=0) in the FORC diagram, indicating all portions of the film experience a bias field. The spread of the FORC feature in

the bias direction is maximal for the d_{CoO}=1.2-1.8 nm sample, showing a very rapid change in exchange field as a function of d_{CoO}. This indicates a change in behavior from fully rotatable CoO to higher anisotropy CoO spins. We also note that the Fe [100] hysteresis loop (Fig. 1a) shows an asymmetry between the descending and ascending branches suggesting irreversible switching inside the CoO.[21, 23] Both the hysteresis in the Fe [010] vector coil loops (Figs. 2c-d, open circles) and the existence of three separate features in the Fe [010] FORC distribution (Fig. 3h) indicate the existence of metastable magnetization states along the Fe [010] and [$0\bar{1}0$] crystalline directions, and a stable state along the Fe [100] direction. This shows the CoO anisotropy is not large enough to overcome the crystalline energy barriers between these states. These metastable states persist until a CoO thickness of d_{CoO}=2.4 nm. This behavior suggests the existence of irreversible switching within the CoO, e.g. a winding-up of a partial domain wall in the AF as suggested by a number of exchange bias models[23, 27] and experiments.[24-26]

Figure 5 shows the family of Fe [100] FORCs as well as the longitudinal hysteresis loops along the Fe [100] and [010] directions. The Fe [100] hysteresis loops (Fig. 5, circles) do not delineate the outer boundary, or "envelope" of the family of FORCs (Fig. 5, lines) as is expected,[53] except for the d_{CoO}>2.4 nm sample (Fig. 5d). A difference between the hysteresis loop and the outer boundary of the FORCs can only occur if the sample is changing states between each reversal curve. In other words, this difference is directly caused by the irreversible switching events occurring within the CoO during the FORC measurement. This change is most evident for d_{CoO}=1.2-1.8 nm (Fig. 5b) in the hysteresis loops measured both prior to and after the FORC measurement procedure. The post-FORC loop is remarkably different from the pre-FORC loop. The post-FORC hysteresis loop is much closer in character to the Fe [010] loop, indicating a massive reorientation of the CoO anisotropy directions. This observation is

analogous to the training effect well documented in exchange biased systems, where typically the AF layer has sufficient anisotropy to establish exchange bias, yet the field cycling is able to modify the AF domains or interfacial pinned AF spins.[55-57] Here the rotatable CoO spins with insufficient anisotropy in the ultrathin layers are responsible for the evolution of hysteresis loops, pointing to a more generic origin of the training effect.

The reorientation during the measurement process manifests itself as a broadening of the FORC features as seen in Fig. 4. The FORC procedure is known to access higher spin disordered states, even in the absence of exchange bias, than the major loop.[58] For the d_{CoO}<1.2 nm samples the effect is much smaller due to the very low anisotropy of the CoO for these thicknesses. Therefore, the FORC distributions shown in Figs. 3-4 correlate well with the major loop magnetometry results shown in Figs. 1-2, even for the CoO thicknesses much thinner than the critical thickness (2.2 nm) where the frozen spins are detectable experimentally.[14] These results reveal details of the magnetization reversal of Fe, suggesting that the irreversible switching events and the rotatable and pinned CoO spins may both contribute to the d_{CoO} dependence of exchange bias and coercivity.

Monte Carlo results

In the experiments, the hysteresis loops measured at 80 K with the field applied along the Fe [010] direction (Fig. 2) have probed the magnetocrystalline cubic Fe [110] energy barrier by analyzing the transverse component of the magnetization. However, exchange bias and coercivity enhancement should be attributed to the stronger energy barriers induced by large uniaxial magnetocrystalline anisotropy of the AF CoO. The anisotropy energy barrier affects individual spins and determines the

spin rigidity, even though these spins are insufficient to form a complete domain. It is conceivable that the exchange bias and coercivity behaviors at the thin AF layer thicknesses may be linked with the energy barriers. Therefore, in the simulations, the energy barriers induced in the AF layer are considered as well. For an AF spin *i*, the energy shown in Eq. (4)-(5) can be rewritten in a Stoner-Wohlfarth form,

$$E_{\mathrm{AF}i} = -K_i^x (S_i^x)^2 - \mathbf{S}_i \cdot (\delta J_{\mathrm{AF}} \sum_{j \in \mathrm{AF}} \mathbf{S}_j + J_{\mathrm{IF}} \sum_{k \in \mathrm{FM}} \mathbf{S}_k + g\mu_{\mathrm{B}} \mathbf{H}) . \quad (6)$$

Divided by K_i^x, it obtains

$$\varepsilon_{\mathrm{AF}i} = -(S_i^x)^2 - 2\mathbf{S}_i \cdot \mathbf{h} , \quad (7)$$

where

$$\mathbf{h} = \frac{\delta J_{\mathrm{AF}} \sum_{j \in \mathrm{AF}} \mathbf{S}_j + J_{\mathrm{IF}} \sum_{k \in \mathrm{FM}} \mathbf{S}_k + g\mu_{\mathrm{B}} \mathbf{H}}{2K_i^x} . \quad (8)$$

The energy barrier is an energy saddle point, which can be calculated by setting the first-order partial derivatives of $\varepsilon_{\mathrm{AF}i}$ with respect to the spin polar (α) and azimuthal (β) angles to zero. Moreover, there exists a critical value ($\mathbf{h}_{\mathrm{C}}$) of **h** to determine whether the energy barrier exists. Fig. 6a illustrates the dependence of $\mathbf{h}_{\mathrm{C}}$ on the angle θ between **h** and easy axis (+**x**). The values of θ can be obtained analytically by solving a quartic equation transformed from $\mathbf{h}_{\mathrm{C}}$.[59] Once θ is determined, the energy curved surface of $\varepsilon_{\mathrm{AF}i}(\alpha,\beta)$ is depicted and thus the value of energy barrier is calculated, e.g. a two-dimensional result of $\varepsilon_{\mathrm{AF}i}$ with β for a given θ is shown in Fig. 6b, where the energy barrier is also indicated. Based on the Néel-Arrhenius relaxation theory, the energy barrier controls the mean time between two spin flips. Hence it is acceptable that the energy barrier influences the Boltzmann flipping probability in the framework of Monte Carlo simulation.[60, 61]

Figure 7 shows the main simulation results of FM hysteresis loops, energy densities, energy barrier densities, and AF spin reversal fractions at the FM/AF interface for small and large AF thicknesses. Note that the spin reversal is defined when the spin rotates over its hard axis under a given magnetic field and that the fraction of spin reversal is quantified by $\rho_r=N_r/N$ where N is the total spin number and N_r is the number of the spins that have reversed at the descending (ascending) field branch starting from H_{+max} (H_{-max}). As shown in Fig. 7a, compared with a single FM layer, a wider hysteresis loop is observed in a FM/AF bilayer with a thin AF layer, and a shift of hysteresis loop towards the negative field direction in a FM/AF bilayer with a thick AF layer, respectively. That is, an enhanced H_C and a negligible H_B are obtained for a thin AF layer similar to the experimental observation for d_{CoO}<1.2 nm. With the increase of the AF layer thickness, H_B appears and increases rapidly while H_C decreases, corresponding to the experimental findings for 1.8 nm<d_{CoO}<3.6 nm. The AF magnetic energy at the FM/AF interface exhibits a symmetric butterfly-like pattern for the thin AF layer (Fig. 7b), indicative of the existence of a uniaxial symmetry instead of a unidirectional one. Moreover, the energy barrier is reversible under high magnetic field (Fig. 7c), in agreement with the discussion by Suess *et al*.[62] The energy barrier is nonlinear with magnetic field due to complex incoherent AF magnetization reversals at the FM/AF interface, and the reversibility indicates that the AF layer with such small thicknesses is not enough to establish the bias via interfacial coupling.[52] The insufficient pinning provided by the thin AF layer is clearly illustrated in Fig. 7d. Over 80% of the AF spins at the FM/AF interface are rotatable under strong magnetic fields, which are stronger than the intrinsic coercive field of the FM layer. Therefore, H_C increases due to magnetic field and interfacial coupling dragging the AF spins to rotate with the FM.[63]

With the increase of the AF layer thickness, the AF anisotropy and exchange interaction are both enhanced. For a large AF layer thickness, the intrinsic anisotropy field may exceed the applied field to stabilize an uncompensated AF interface layer and thus breaks the uniaxial symmetry of the energy with magnetic field (Fig. 7b). At low temperature, the energy barrier is dependent on magnetic field direction, i.e. it is lower when the magnetic field is positive. With the decrease of the magnetic field, the energy barrier is reduced. Interestingly, the FM magnetization reversal occurs only when the AF anisotropy energy barrier is reduced to smaller than zero, and the FM magnetization reversal induces a sudden drop of the energy barrier. However, it fails to predict the FM magnetization reversal from the energy barrier value explicitly. In addition, with the decrease of the magnetic field in the positive direction, the AF spin reversal occurs at the FM/AF interface due to AF exchange interaction, not magnetic field. The reconstruction of the AF spin configuration at the FM/AF interface decreases the net AF magnetization and the AF anisotropy energy barrier, favoring the FM magnetization reversal to occur under a smaller magnetic field. When the magnetic field begins to decrease in the negative direction, the AF layer keeps higher energy and energy barrier. The high energy indicates the existence of a large net positive magnetization, and the high energy barrier impedes the AF spin reversal. Therefore, the FM magnetization reversal is favored under a much smaller magnetic field, leading to a large shift of the hysteresis loop towards the negative field direction. As shown in Fig. 7d, the total number of the spins that have reversed are converging for the descending and ascending field branches, indicating that the fractions of the rotatable and pinned spins are determined by the AF layer thickness only. However, different energies and energy barriers for the two field sweep branches cause the spin reversals to occur under different magnetic fields and thus giving rise to exchange bias. Therefore, the simulation results

demonstrate that, for the thin AF layer, the anisotropy energy barrier is high enough to stabilize the AF spins under weak fields, while they may be overcome by strong fields. The rotatable spins contributing to the coercivity enhancement originate from the magnetic field rather than incomplete AF domains. That is, the phenomenon of a large H_C associated with a small H_B for the small d_{CoO} originates from many rotatable spins at the CoO interface that are mainly driven by the magnetic field. When the AF layer thickness increases, the AF anisotropy energy is enhanced and some AF spins may be trapped in one of the easy-axis directions by high anisotropy energy barriers during FM magnetization reversal, and the symmetries of the FM spin reversals at the two field sweep branches are broken due to FM/AF interfacial coupling. Therefore, the pronounced H_B and the reduced H_C for the large d_{CoO} are dynamically formed and attributed to the AF spins at the FM/AF interface that are frozen in a preferred direction by high anisotropy.

Summary

We have investigated the onset of exchange bias and coercivity enhancement in epitaxial CoO/Fe/MgO(100) films with ultrathin AF thickness, even before frozen CoO spins are detected. Vector magnetometry and FORC studies reveal different CoO thickness dependence of the exchange bias and coercivity enhancement. Interestingly, coexistence of a high coercivity, low bias phase and a high bias, low coercivity phase is revealed as the magnetization reversal evolves from being influenced by rotatable CoO moments to frozen CoO moments. The AF domain state is found to be metastable, which can be reoriented by external and exchange fields prior to the appearance of frozen spins. This is manifested in the evolution of FORC distributions, both the peak positions and the extent of the distributions, and the

massive training-type effect seen before and after the FORC measurement. Simulations by means of a modified Monte Carlo method also agree well with these experimental observations, and show that the AF anisotropy energy barrier and the rotatable spins induced by magnetic field and exchange interaction at the interface are responsible for the observed effects.

Acknowledgements

This contribution is dedicated to Professor Chia-Ling Chien, on the occasion of his 80th birthday. Prof. Chien's numerous original contributions to the field of magnetism, spintronics and superconductivity, as well as his tireless service to the magnetism community, have inspired generations of scientists, the authors included. K.L. has been privileged to be a beneficiary of Prof. Chien's wisdom, mentorship and support over the years. We thank J. S. Park for assistance with sample preparation. This work has been supported by the NSF DMR-1610060 (UCD) and DMR-2005108 (GU). Work at UCB supported by the US Department of Energy, Office of Science, Office of Basic Energy Sciences, Materials Sciences and Engineering Division under Contract No. DE-AC02-05CH11231 (van der Waals heterostructures program, KCWF16).

References

* Electronic-mail: kai.liu@georgetown.edu.

[1] W. H. Meiklejohn and C. P. Bean, Phys. Rev. **102**, 1413 (1956).

[2] J. Nogués and I. K. Schuller, J. Magn. Magn. Mater. **192**, 203 (1999).

[3] A. E. Berkowitz and K. Takano, J. Magn. Magn. Mater. **200**, 552 (1999).

[4] R. L. Stamps, J. Phys. D: Appl. Phys. **33**, R247 (2000).

[5] M. Kiwi, J. Magn. Magn. Mater. **234**, 584 (2001).

[6] B. Dieny, V. S. Speriosu, S. S. P. Parkin, B. A. Gurney, D. R. Wilhoit, and D. Mauri, Phys. Rev. B **43**, 1297 (1991).

[7] W. G. Wang, M. G. Li, S. Hageman, and C. L. Chien, Nat. Mater. **11**, 64 (2012).

[8] J. Nogues, J. Sort, V. Langlais, V. Skumryev, S. Surinach, J. S. Munoz, and M. D. Baro, Phys. Rep. **422**, 65 (2005).

[9] S. D. Bader, Rev. Mod. Phys. **78**, 1 (2006).

[10] S. M. Zhou, K. Liu, and C. L. Chien, Phys. Rev. B **58**, R14717 (1998).

[11] X. He, Y. Wang, N. Wu, A. N. Caruso, E. Vescovo, K. D. Belashchenko, P. A. Dowben, and C. Binek, Nat. Mater. **9**, 579 (2010).

[12] S. Manipatruni, D. E. Nikonov, C.-C. Lin, B. Prasad, Y.-L. Huang, A. R. Damodaran, Z. Chen, R. Ramesh, and I. A. Young, Sci. Adv. **4**, eaat4229 (2018).

[13] D. A. Gilbert, J. Olamit, R. K. Dumas, B. J. Kirby, A. J. Grutter, B. B. Maranville, E. Arenholz, J. A. Borchers, and K. Liu, Nat. Commun. **7**, 11050 (2016).

[14] L. Wei, Z. Hu, G. Du, Y. Yuan, J. Wang, H. Tu, B. You, S. Zhou, J. Qu, H. Liu, R. Zheng, Y. Hu, and J. Du, Adv. Mater. **30**, 1801885 (2018).

[15] J. Zehner, R. Huhnstock, S. Oswald, U. Wolff, I. Soldatov, A. Ehresmann, K. Nielsch, D. Holzinger, and K. Leistner, Adv. Electron. Mater. **5**, 1900296 (2019).

[16] P. D. Murray, C. J. Jensen, A. Quintana, J. W. Zhang, X. X. Zhang, B. J. Kirby, and K. Liu, ACS Appl. Mater. Interfaces **13**, 38916 (2021).

[17] C. J. Jensen, A. Quintana, M. Sallb, L. Herrera-Diez, X. X. Zhang, D. Ravelosona, and K. Liu, J. Magn. Magn. Mater. **540**, 168479 (2021).

[18] M. Huang, M. U. Hasan, K. Klyukin, D. Zhang, D. Lyu, P. Gargiani, M. Valvidares, S. Sheffels, A. Churikova, F. Büttner, J. Zehner, L. Caretta, K.-Y. Lee, J. Chang, J.-P. Wang, K. Leistner, B. Yildiz, and G. S. D. Beach, Nat. Nanotechnol. **16**, 981 (2021).

[19] T. Ambrose and C. L. Chien, Phys. Rev. Lett. **76**, 1743 (1996).

[20] F. Y. Yang and C. L. Chien, Phys. Rev. Lett. **85**, 2597 (2000).

[21] R. Morales, Z. P. Li, J. Olamit, K. Liu, J. M. Alameda, and I. K. Schuller, Phys. Rev. Lett. **102**, 097201 (2009).

[22] C. Binek, A. Hochstrat, and W. Kleemann, J. Magn. Magn. Mater. **234**, 353 (2001).

[23] D. Mauri, H. C. Siegmann, P. S. Bagus, and E. Kay, J. Appl. Phys. **62**, 3047 (1987).

[24] N. J. Gökemeijer, J. W. Cai, and C. L. Chien, Phys. Rev. B **60**, 3033 (1999).

[25] C. L. Chien, V. S. Gornakov, V. I. Nikitenko, A. J. Shapiro, and R. D. Shull, Phys. Rev. B **68**, 014418 (2003).

[26] Z. P. Li, O. Petracic, R. Morales, J. Olamit, X. Batlle, K. Liu, and I. K. Schuller, Phys. Rev. Lett. **96**, 217205 (2006).

[27] M. Stiles and R. McMichael, Phys. Rev. B **59**, 3722 (1999).

[28] J. Keller, P. Miltenyi, B. Beschoten, G. Guntherodt, U. Nowak, and K. D. Usadel, Phys. Rev. B **66** (2002).

[29] P. Miltényi, M. Gierlings, J. Keller, B. Beschoten, G. Güntherodt, U. Nowak, and K. D. Usadel, Phys. Rev. Lett. **84**, 4224 (2000).

[30] J.-I. Hong, T. Leo, D. J. Smith, and A. E. Berkowitz, Phys. Rev. Lett. **96**, 117204 (2006).

[31] M. Fecioru-Morariu, S. R. Ali, C. Papusoi, M. Sperlich, and G. Güntherodt, Phys. Rev. Lett. **99**, 097206 (2007).

[32] U. Nowak, K. D. Usadel, J. Keller, P. Miltényi, B. Beschoten, and G. Güntherodt, Phys. Rev. B **66**, 014430 (2002).

[33] J. Wu, J. S. Park, W. Kim, E. Arenholz, M. Liberati, A. Scholl, Y. Z. Wu, C. Hwang, and Z. Q. Qiu, Phys. Rev. Lett. **104**, 217204 (2010).

[34] Y. Meng, J. Li, P. A. Glans, C. A. Jenkins, E. Arenholz, A. Tan, J. Gibbons, J. S. Park, C. Hwang, H. W. Zhao, and Z. Q. Qiu, Phys. Rev. B **85**, 014425 (2012).

[35] J. Li, Y. Meng, J. S. Park, C. A. Jenkins, E. Arenholz, A. Scholl, A. Tan, H. Son, H. W. Zhao, C. Hwang, Y. Z. Wu, and Z. Q. Qiu, Phys. Rev. B **84**, 094447 (2011).

[36] D. Giannotti, H. Hedayat, G. Vinai, A. Picone, A. Calloni, G. Berti, M. Riva, G. Bussetti, F. Boschini, P. Torelli, G. Panaccione, E. Carpene, C. Dallera, M. Finazzi, and A. Brambilla, Appl. Phys. Lett. **109**, 232401 (2016).

[37] Q. Li, G. Chen, T. P. Ma, J. Zhu, A. T. N'Diaye, L. Sun, T. Gu, Y. Huo, J. H. Liang, R. W. Li, C. Won, H. F. Ding, Z. Q. Qiu, and Y. Z. Wu, Phys. Rev. B **91**, 134428 (2015).

[38] J. Miguel, R. Abrudan, M. Bernien, M. Piantek, C. Tieg, J. Kirschner, and W. Kuch, J. Phys. Condens. Matter **21**, 185004 (2009).

[39] R. Bali, M. M. Soares, A. Y. Ramos, H. C. N. Tolentino, F. Yildiz, C. Boudot, O. Proux, M. D. Santis, M. Przybylski, and J. Kirschner, Appl. Phys. Lett. **100**, 132403 (2012).

[40] C. R. Pike, A. P. Roberts, and K. L. Verosub, J. Appl. Phys. **85**, 6660 (1999).

[41] J. E. Davies, O. Hellwig, E. E. Fullerton, G. Denbeaux, J. B. Kortright, and K. Liu, Phys. Rev. B **70**, 224434 (2004).

[42] M. T. Rahman, R. K. Dumas, N. Eibagi, N. N. Shams, Y.-C. Wu, K. Liu, and C.-H. Lai, Appl. Phys. Lett. **94**, 042507 (2009).

[43] D. A. Gilbert, G. T. Zimanyi, R. K. Dumas, M. Winklhofer, A. Gomez, N. Eibagi, J. L. Vicent, and K. Liu, Sci. Rep. **4**, 4204 (2014).

[44] D. A. Gilbert, B. B. Maranville, A. L. Balk, B. J. Kirby, P. Fischer, D. T. Pierce, J. Unguris, J. A. Borchers, and K. Liu, Nat. Commun. **6**, 8462 (2015).

[45] E. C. Burks, D. A. Gilbert, P. D. Murray, C. Flores, T. E. Felter, S. Charnvanichborikarn, S. O. Kucheyev, J. D. Colvin, G. Yin, and K. Liu, Nano Lett. **21**, 716 (2021).

[46] J. Olamit, K. Liu, Z. P. Li, and I. K. Schuller, Appl. Phys. Lett. **90**, 032510 (2007).

[47] M. Ali, C. H. Marrows, and B. J. Hickey, Phys. Rev. B **67**, 172405 (2003).

[48] H. Xi and R. M. White, Phys. Rev. B **61**, 80 (2000).

[49] J. Moritz, P. Bacher, and B. Dieny, Phys. Rev. B **90**, 024429 (2014).

[50] A. G. Biternas, R. W. Chantrell, and U. Nowak, Phys. Rev. B **89**, 184405 (2014).

[51] H. Sang, Y. W. Du, and C. L. Chien, J. Appl. Phys. **85**, 4931 (1999).

[52] M. S. Lund, W. A. A. Macedo, K. Liu, J. Nogues, I. K. Schuller, and C. Leighton, Phys. Rev. B **66**, 054422 (2002).

[53] R. K. Dumas, C. P. Li, I. V. Roshchin, I. K. Schuller, and K. Liu, Phys. Rev. B **75**, 134405 (2007).

[54] J. Olamit and K. Liu, J. Appl. Phys. **101**, 09E508 (2007).

[55] S. Brems, D. Buntinx, K. Temst, C. Van Haesendonck, F. Radu, and H. Zabel, Phys. Rev. Lett. **95**, 157202 (2005).

[56] E. Menéndez, T. Dias, J. Geshev, J. F. Lopez-Barbera, J. Nogués, R. Steitz, B. J. Kirby, J. A. Borchers, L. M. C. Pereira, A. Vantomme, and K. Temst, Phys. Rev. B **89**, 144407 (2014).

[57] H.-L. Liu, S. Brems, Y.-J. Zeng, K. Temst, A. Vantomme, and C. Van Haesendonck, Phys. Rev. B **90**, 214402 (2014).

[58] R. K. Dumas, P. K. Greene, D. A. Gilbert, L. Ye, C. Zha, J. Åkerman, and K. Liu, Phys. Rev. B **90**, 104410 (2014).

[59] X. Chi, W. Rui, J. Du, S. Zhou, A. Du, and Y. Hu, Appl. Phys. Lett. **108**, 172401 (2016).

[60] Y. Hu and A. Du, Phys. Status Solidi B **248**, 2932 (2011).

[61] D. P. Landau and K. Binder, (Cambridge University Press, Cambridge, 2000), p. 71.

[62] D. Suess, J. Fidler, G. Zimanyi, T. Schrefl, and P. Visscher, Appl. Phys. Lett. **92**, 173111 (2008).

[63] C. Leighton, J. Nogués, B. J. Jönsson-Åkerman, and I. K. Schuller, Phys. Rev. Lett. **84**, 3466 (2000).

Figure Captions

FIG. 1. Longitudinal hysteresis loops of Fe(10nm)/CoO(d_{CoO}) films with different CoO thickness measured along the Fe [100], the field cooling axis, cooled and measured at 80 K, as illustrated in the schematic. Loops for d_{CoO}<2.4 nm exhibit asymmetric character, with pronounced differences between the ascending and descending-field branches.

FIG. 2. Longitudinal (solid circles) and transverse (open circles) hysteresis loops of Fe(10nm)/CoO(d_{CoO}) films with different CoO thickness measured at 80 K. Schematic shows the experimental geometry, with the measurement field applied along the Fe [010] direction, field cooling performed along the Fe [100] direction.

FIG. 3. FORC distributions measured at 77 K are shown with cooling field along the Fe [100] direction for applied field along the Fe [100] and Fe [010] directions. Fe [100] FORC distributions show the evolution of bias and coercivity as a function of d_{CoO}. Fe [010] FORCs show the evolution of the exchange anisotropy versus the crystalline anisotropy.

FIG. 4. Evolution of the FORC distribution in H_C and H_B (solid symbols) and the half-width-at-half-maximum (HWHM) of each integrated FORC distribution (open symbols) as a function of d_{CoO}. The HWHMs for the features are maximal just below the thickness where frozen CoO spins are observed and are indicative of irreversible switching events within the CoO.

FIG. 5. Selected families of FORCs along with longitudinal hysteresis loops. The outer boundary of the FORCs are significantly different from the pre-FORC hysteresis loops for d_{CoO}<2.4 nm. At d_{CoO}=1.2-1.8 nm the post-FORC hysteresis loop shows nearly zero bias and is very similar to the Fe [010] loop.

FIG. 6. (a) Normalized critical effective field as a function of the angle (θ) between the effective field and the easy axis in the +*x* direction. (b) Spin energy as a function of the spin azimuthal angle (β) under different normalized effective fields with θ = 57.3°, where the spin energy involves a magnetocrystalline anisotropy energy of an individual spin, and exchange and Zeeman energies of this spin coupled with its nearest neighbors and an external magnetic field, and the spin azimuthal angle is between the projection of the spin in the *xy* plane and the +*x* axis. A schematic illustration of the directions of easy axis, effective field and spin is also shown in (a).

FIG. 7. (a) Calculated FM hysteresis loops without the AF layer (0M AF) or in the FM/AF bilayers with one-monolayer (1M)/seven-monolayer (7M) AF layer thickness at low temperature. (b-d) AF energy density (ε), AF energy barrier density (ε^b), and fraction of rotatable AF spin (ρ_r) at the FM/AF interface as a function of applied field. Here the energy density is the energy per AF spin at the FM/AF interface obtained from the simulation, the energy barrier density is the secondary maximum value of the 4π-space energy per AF spin at the FM/AF interface calculated analytically, and the fraction ρ_r is the result of the number of rotatable AF spins divided by the total number of AF spins at the FM/AF interface. Red circles and blue triangles denote the results obtained in the FM/AF bilayers with one-monolayer (1M) and seven-monolayer (7M) AF layer thicknesses, respectively. Solid and dashed arrows point out the magnetizing directions at the descending (solid symbols) and ascending (open symbols) field branches.

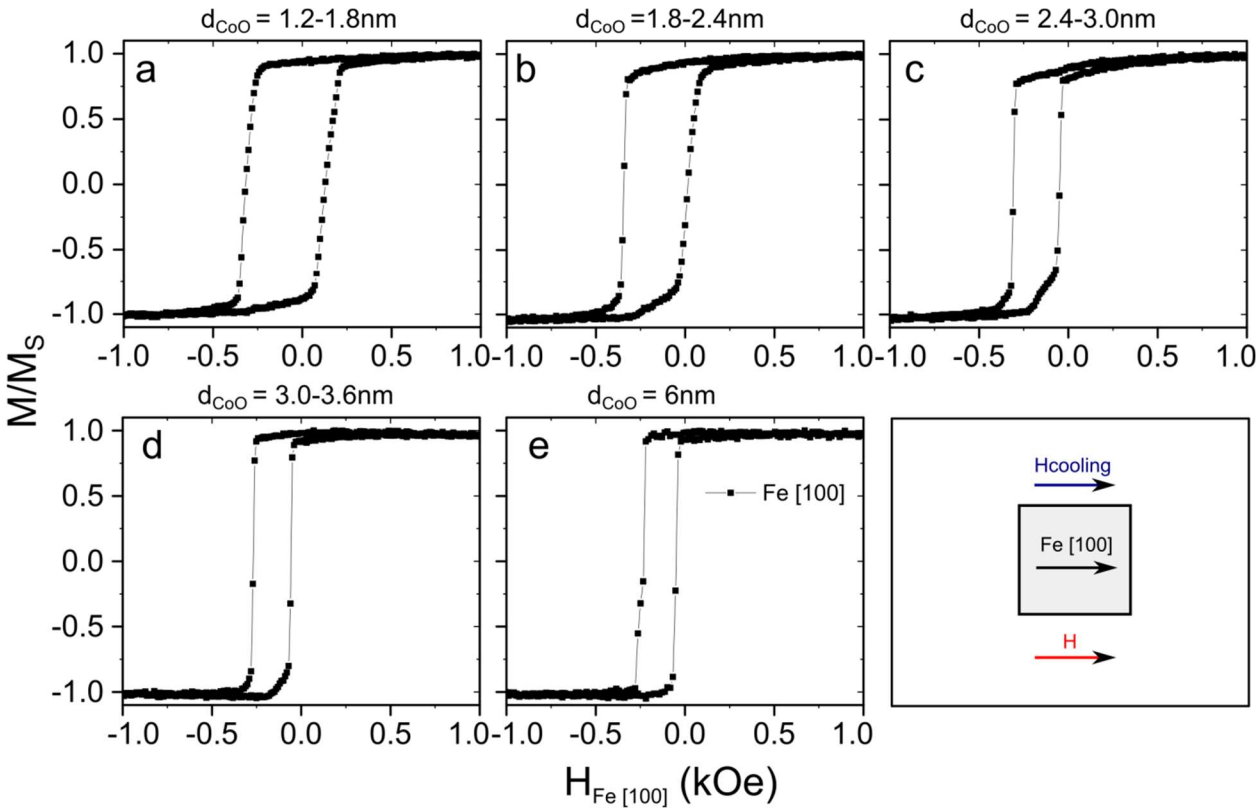
d_{CoO} = 1.2-1.8nm
d_{CoO} =1.8-2.4nm
d_{CoO} = 2.4-3.0nm
d_{CoO} = 3.0-3.6nm
d_{CoO} = 6nm
a
b
c
d
e
M/M$_S$
$H_{Fe\ [100]}$ (kOe)
Fe [100]
Hcooling
Fe [100]
H

Figure 1.

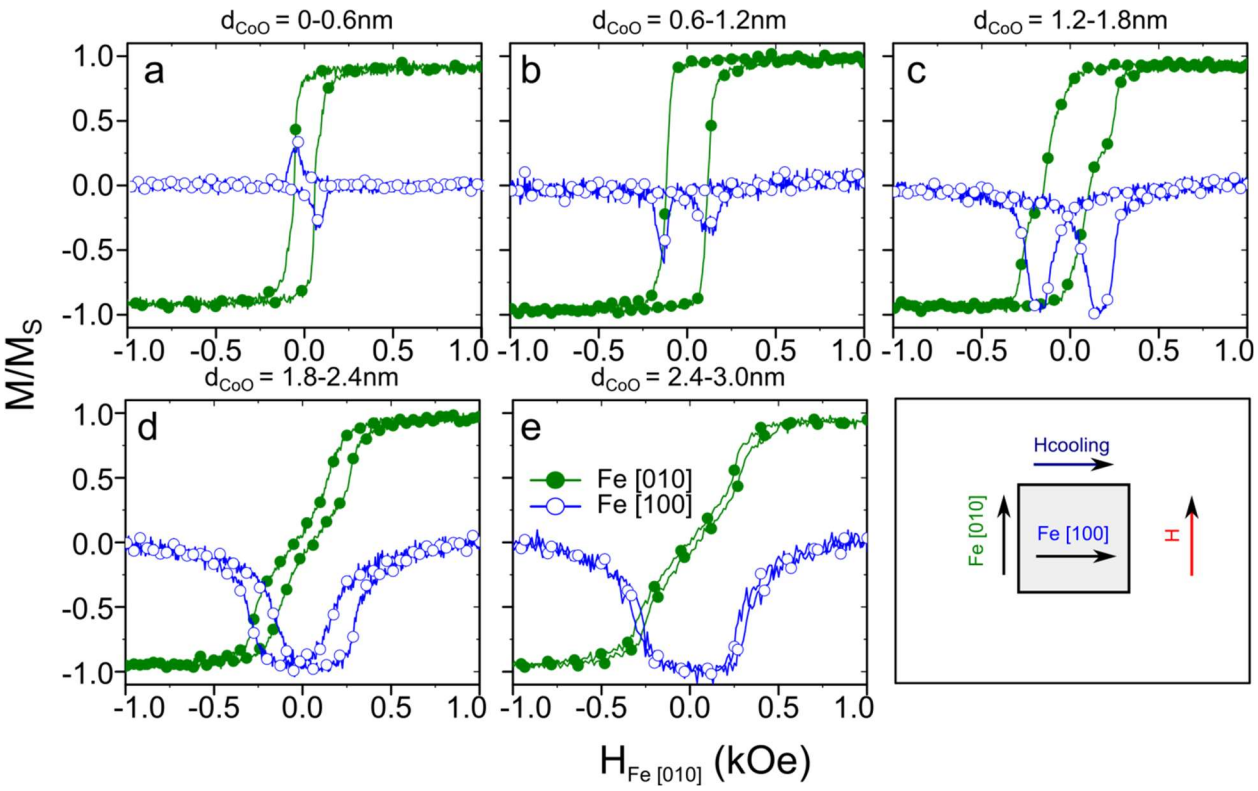
d_CoO = 0-0.6nm
d_CoO = 0.6-1.2nm
d_CoO = 1.2-1.8nm
d_CoO = 1.8-2.4nm
d_CoO = 2.4-3.0nm
a
b
c
d
e
M/M_S
H_Fe [010] (kOe)
Fe [010]
Fe [100]
Hcooling
Fe [010]
Fe [100]
H

Figure 2.

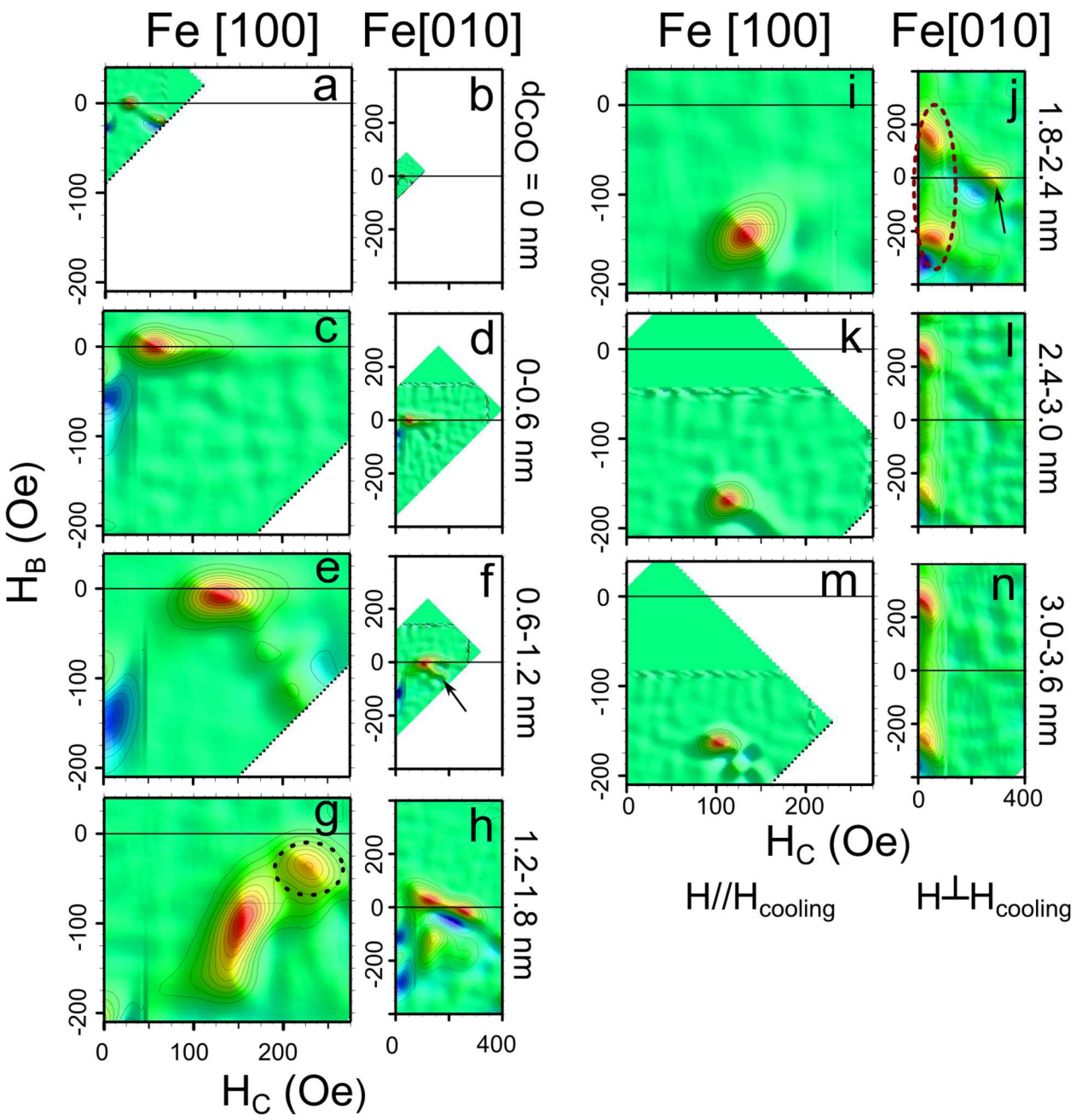
Fe [100]
Fe[010]
Fe [100]
Fe[010]
a
b
c
d
e
f
g
h
i
j
k
l
m
n
d_{CoO} = 0 nm
0-0.6 nm
0.6-1.2 nm
1.2-1.8 nm
1.8-2.4 nm
2.4-3.0 nm
3.0-3.6 nm
H_B (Oe)
H_C (Oe)
H_C (Oe)
H//$H_{cooling}$
H⊥$H_{cooling}$

Figure 3.

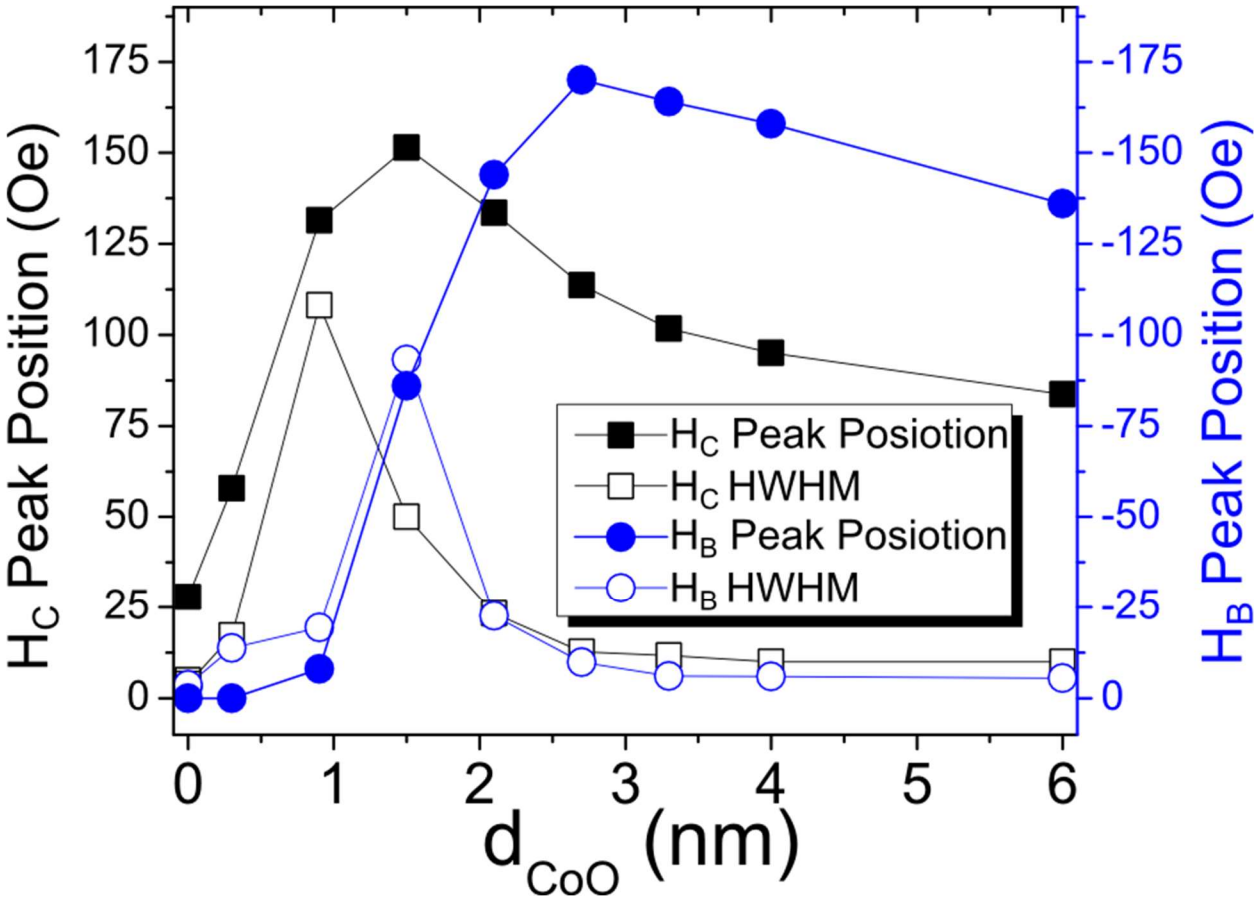
H_C Peak Position (Oe)
H_B Peak Position (Oe)
d_CoO (nm)
H_C Peak Posiotion
H_C HWHM
H_B Peak Posiotion
H_B HWHM
175
150
125
100
75
50
25
0
-175
-150
-125
-100
-75
-50
-25
0
0
1
2
3
4
5
6

Figure 4.

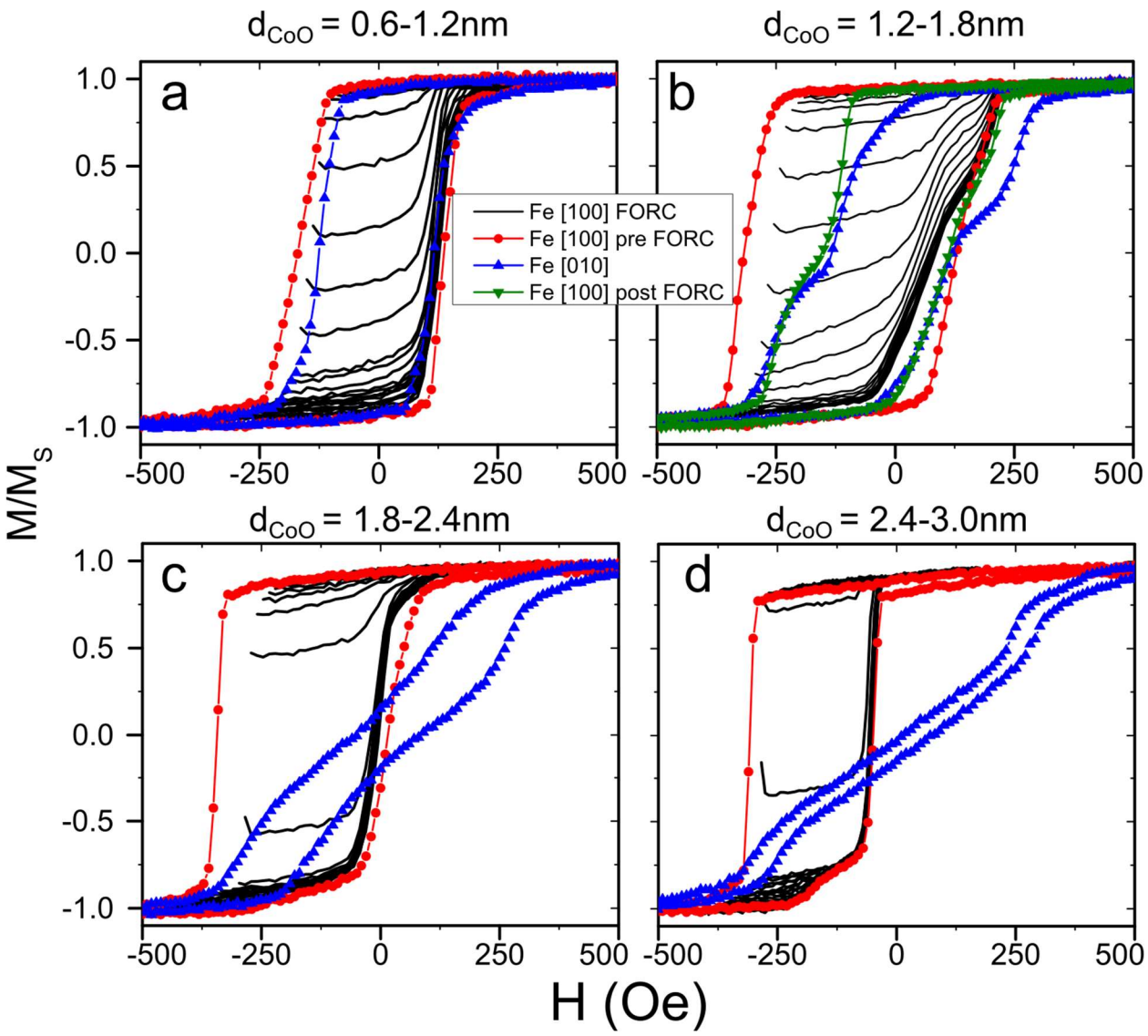
d$_{CoO}$ = 0.6-1.2nm
d$_{CoO}$ = 1.2-1.8nm
d$_{CoO}$ = 1.8-2.4nm
d$_{CoO}$ = 2.4-3.0nm
a
b
c
d
Fe [100] FORC
Fe [100] pre FORC
Fe [010]
Fe [100] post FORC
M/M$_S$
H (Oe)
1.0
0.5
0.0
-0.5
-1.0
-500
-250
0
250
500

Figure 5.

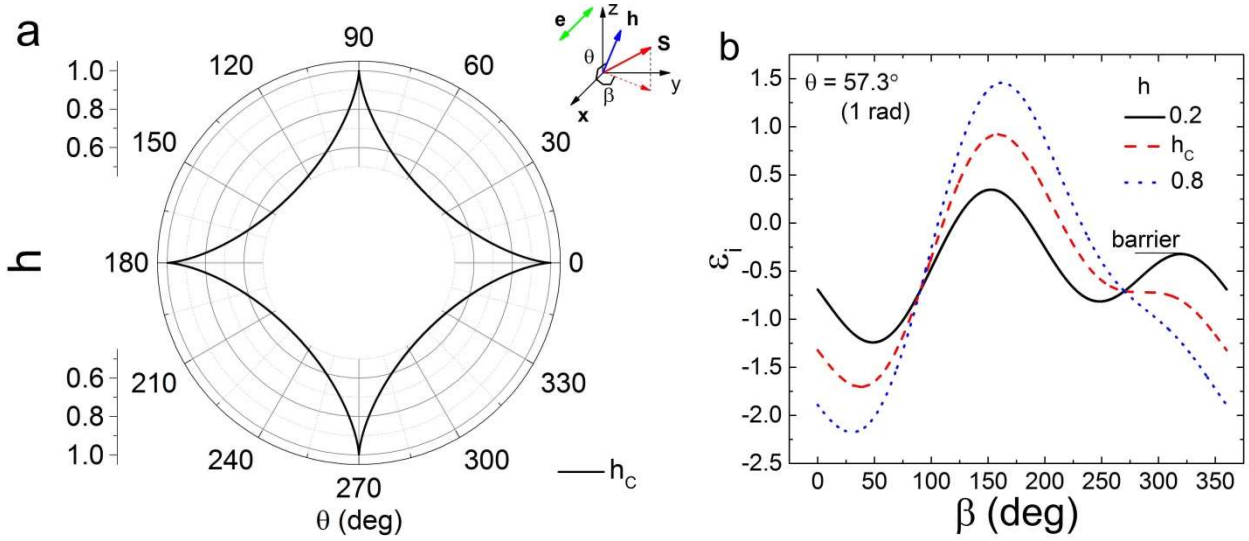
a
b
h
θ (deg)
β (deg)
ε_i
h_C
θ = 57.3°
(1 rad)
h
0.2
h_C
0.8
barrier
e
z
h
s
θ
β
x
y

Figure 6.

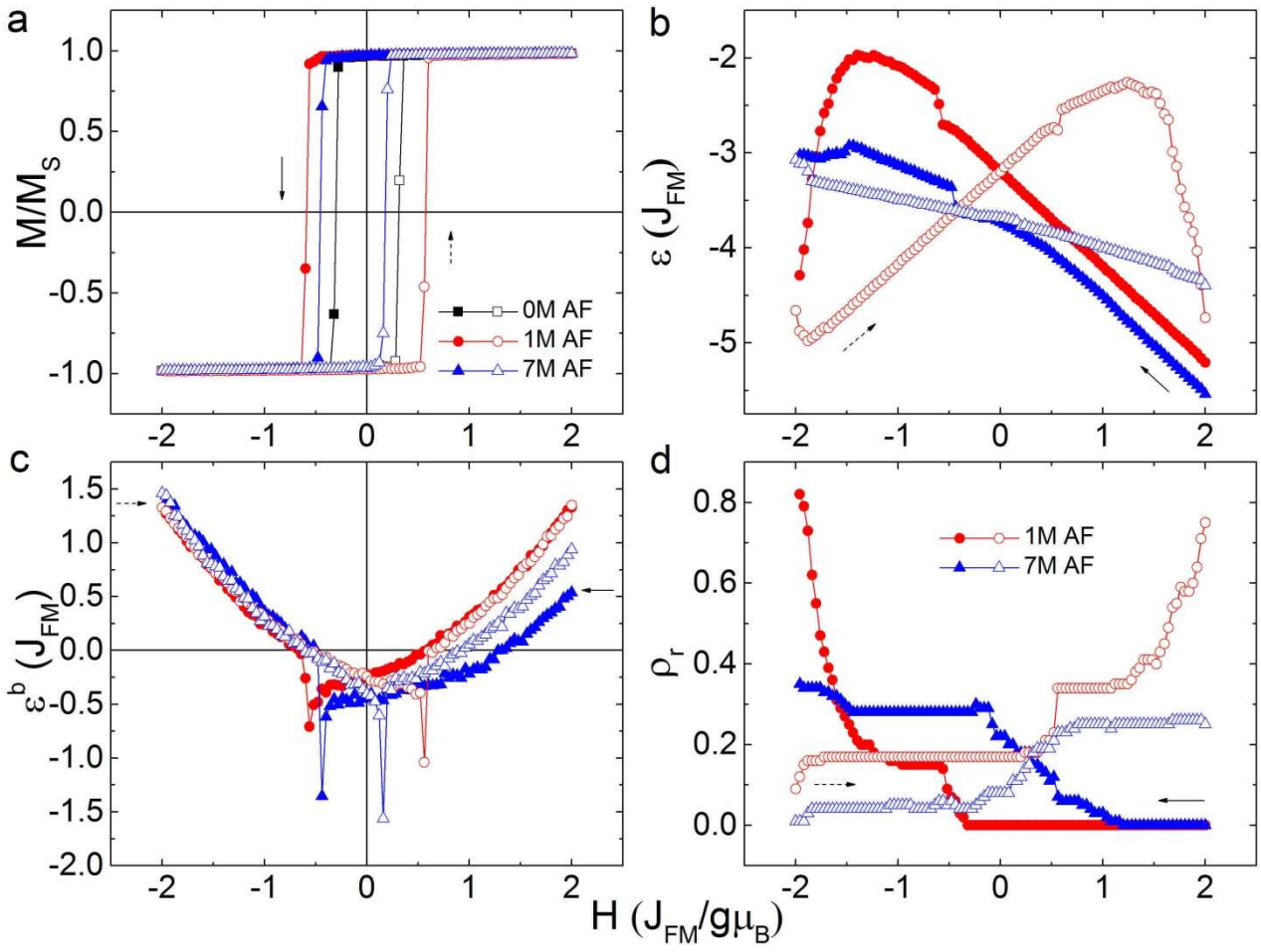

Figure 7.

Table 1. Values of parameters used in the simulation.

	K^x	K^y	K^z	J	δ	p	$H_{\max}$	T
FM	0.1	0.05	-0.1	1.0	_	_	2.0	0.1
Thin AF	3.05	0	0	-0.5δ	0 or 1	0		
Thick AF	3.70	0	0	-0.5δ		0.34		

K and J are the anisotropy and exchange interaction constants in unit of energy (J_{FM}).

δ equals 0 or 1 determined by the bonding fraction p of AF coupling.

$H_{\max}$ is the maximum measuring field value in unit of $J_{\mathrm{FM}}/g\mu_{\mathrm{B}}$.

T is the temperature in unit of $J_{\mathrm{FM}}/k_{\mathrm{B}}$.